AD-A033 584 NAVY MARINE ENGINEERING LAB ANNAPOLIS MD F/G 20/2
ATOMIC ORDERING IN BINARY A15-TYPE PHASES.(U)
MAR 67 E C VAN REUTH , R M WATERSTRAT
UNCLASSIFIED MEL-6/67 NL

END

DATE FILMED 2-77

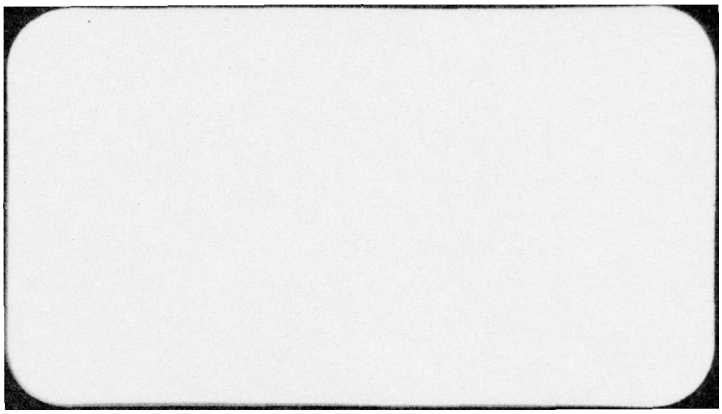

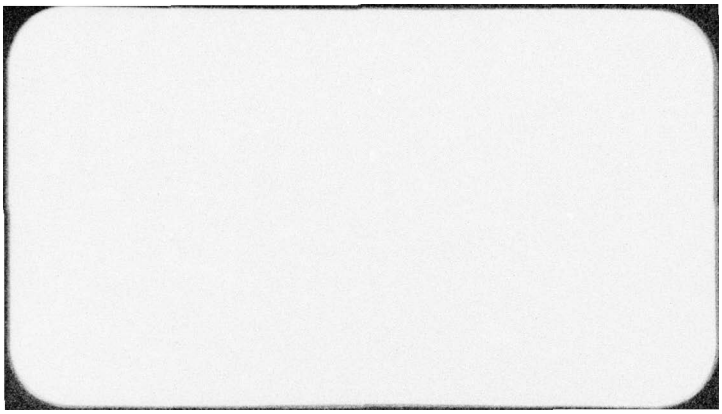

Atomic Ordering in Binary A15-Type Phases

Assignment 87 121
MEL R&D Phase Report 6/67
March 1967

By
E. C. van Reuth
and
R. M. Waterstrat

R. M. Waterstrat
R. M. WATERSTRAT

E. C. van Reuth
E. C. VAN REUTH

Approved by:

W. L. Williams
W. L. WILLIAMS
Naval Alloys Division

Distribution List

NAVSHIPS (SHIPS 0342)
NAVSHIPS (SHIPS 03422)
NAVSHIPS (SHIPS 2021) (2)
NAVSEC (SEC 6101)
CO, ONR, London (2)
ONR
DTMB
DDC (20)
DNL
NAVSECPHILADIV
Addressee (6)

ABSTRACT

The degree of long-range order has been determined for 20 binary A15-type phases containing various transition elements. A tendency toward a lower degree of order was noted as the component elements were chosen successively from columns in the periodic table approaching the Mn column. A comparison of the ordering in the A15-type phases with the ordering previously reported for various binary sigma phases suggests that the remarkable stability of these phases may result from an interdependence between the electronic structure and the ability of the atoms to undergo deformations in conforming to geometrical packing requirements.

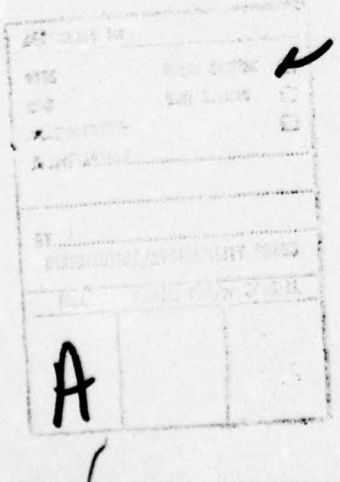

ADMINISTRATIVE INFORMATION

This investigation is supported by the Foundational Research Program, Sub-project Z-R011 01 01, Task 0401.

TABLE OF CONTENTS

	Page
DISTRIBUTION LIST	ii
ABSTRACT	iii
ADMINISTRATIVE INFORMATION	iv
EXPERIMENTAL PROCEDURE	3
Alloy Preparation	3
X-ray Diffraction	7
Model Calculations	11
EXPERIMENTAL RESULTS	14
DISCUSSION	27
ACKNOWLEDGMENTS	35
REFERENCES	37

LIST OF FIGURES

Figure 1 - X-ray Pattern of a Highly Ordered A15-Type Phase (Ti_3Pt) Compared With the Pattern of a Partially Disordered A15-Type Phase ($Cr_{72}Os_{28}$)

Figure 2 - Degree of Atomic Ordering in A15-Type Phases as a Function of the Position of the Constituent Elements in the Periodic Table

Figure 3 - A-A Lattice Contractions in A15-Type Phases as a Function of the Goldschmidt Radius Ratio (R_A/R_B)

Figure 4 - Atomic Configuration Occurring in Both the Sigma Phases and the A15-Type Phases

APPENDIXES

Appendix A - Nomenclature (6 pages)

Atomic Ordering in Binary A15-Type Phases

E. C. van Reuth and R. M. Waterstrat

A common crystallographic feature of many alloy phases formed by the transition elements is the occurrence of tetrahedral groupings of atoms throughout the structure. When the atoms in such a structure differ in size by less than 25 percent, considerable justification may be obtained for the existence of four characteristic coordination polyhedra (Kaspar polyhedra) each having triangular faces and possessing coordination numbers of 12, 14, 15, and 16, respectively, (Kasper, 1956; Frank and Kasper, 1958, 1959). The icosahedral 12-coordinated polyhedron would appear to be an appropriate site for the smaller atoms in the structure, while the sites with 14, 15, or 16, coordinations would seem to be most appropriate for the larger atoms. If atomic packing considerations are an important factor in stabilizing these phases, one might therefore expect an atomic ordering to occur. Such an ordering of atoms has been observed in many of these structures, and in some cases it has been possible to measure the extent of atomic ordering on each crystallographic lattice site. Unfortunately, the accuracy of these measurements has often been restricted by the necessity of simultaneously determining the atomic position parameters.

In the A15-structure type, however, the atomic position parameters are fixed by the symmetry requirements of space group Pm3n (Table 1). Consequently, measurements of atomic ordering in these phases can be interpreted more accurately and with less ambiguity, since there are only two crystallographic lattice sites.

Table 1

Space Group, Atomic Positions and

Atomic Coordination Numbers for the A15-Type Structure

(A_3B) Space Group Pm3n

Atom type	Number of atoms per unit cell	Atom Positions	Coordination Number
6(c)	6	0, 1/4, 1/2	14
		0, 3/4, 1/2	
		1/2, 0, 1/4	
		1/2, 0, 3/4	
		1/4, 1/2, 0	
		3/4, 1/2, 0	
2(a)	2	0, 0, 0	12
		1/2, 1/2, 1/2	

Geller, Matthias, and Goldstein, (1955); have reported a high degree of atomic ordering in Nb_3Os, Nb_3Ir, Nb_3Pt, and V_3Sn but only a partial ordering in Ta_3Sn. The partial ordering in Ta_3Sn has recently been confirmed by Courtney, Pearsall, and Wulff, (1965a); who have also reported evidence that vacant atomic sites exist in this phase after a vacuum heat treatment. Matthias, Geballe, Willens, Corenzwit, and Hull, (1965); have produced a considerable amount of disorder in the phase Nb_3Ge by using special rapid-quenching techniques.

In view of the considerable practical interest in the A15-type phases as superconductors with exceptionally high transition temperatures (Matthias, 1963), it is remarkable that only this rather limited amount of information is available in the literature concerning detailed studies of the extent of

atomic ordering in these phases. In many instances the A15-type phases have apparently been assumed to be completely ordered since their composition ranges of stability are relatively narrow and frequently confined to the so-called "ideal" composition (A_3B). The recent discoveries of binary A15-type phases which are stable at compositions deviating significantly from the "ideal" (A_3B) composition (Darby and Zegler, 1962; Hartly, Parsons, and Seedly, 1964; Ray and Parsons, 1966; Sadogopan, Gatos, and Giessen, 1965; Raub and Röschel, 1966) suggest that the crystallographic sites in this structure need not be occupied exclusively by only one chemical element.

Evidence presented in this paper indicates that many of the A15-type phases possess rather incomplete atomic ordering. In some cases a substantial fraction of the atoms of a given element may occupy both crystallographic lattice sites even when the composition of the phase corresponds closely to the "ideal" (A_3B) stoichiometric composition (Waterstrat and van Reuth, 1966).

This study of the atomic ordering in twenty binary A15-type phases was undertaken primarily to ascertain those factors which may be responsible for the atomic ordering and which may perhaps also be responsible for the remarkable stability of the A15-type phases.

EXPERIMENTAL PROCEDURE

Alloy Preparation

All alloys reported here except the Mo-Pt (specimen No. 1 only), Cr-Os (specimen No. 1 only), and Cr-Pt (specimen No. 1 only) were melted in an inert gas arc-melting furnace. The constituent metals had the nominal purities shown in Table 2. Each arc-melted specimen was melted at least four times and was inverted between each melting. Melting weight losses were always less than one percent.

Table 2

Purity of Metals Used in Alloy Preparation

Metal	Purity, %
Titanium	99.9
Vanadium	99.95
Chromium	99.999
Niobium	99.9
Molybdenum	99.9
Rhodium	99.95
Osmium	99.999
Iridium	99.95
Platinum	99.99
Gold	99.99
Ruthenium	99.9
Palladium	99.9

The Mo-Pt (specimen No. 1), Cr-Os (speciment No. 1), and Cr-Pt (specimen No. 1) alloys were prepared by powder metallurgy techniques. Powders having a minimum purity of 99.9 percent and a 20-50 micron particle size were thoroughly mixed in the proper proportions and compressed in a 1/2-inch diameter cylindrical die at a pressure of 50,000 psi. These green compacts were then sintered for 48, 8 and 9 hours, respectively, at temperatures of 1600 C, 1400 C, and 1300 C, respectively. The weight losses during sintering of these alloys were between one and four percent. However, in these samples, the losses were confined to a thin surface layer which was subsequently removed.

All annealing treatments were conducted in a vacuum furnace using tantalum heating elements. During the annealing treatments a pressure of 10^{-6} to 10^{-7} torr was maintained. The annealing furnace was calibrated by a thermocouple and an optical pyrometer jointly whenever possible and separately at high (>1600 C) or low temperatures (<1000 C). The annealing treatments used for each alloy specimen are given in Table 3.

Table 3

Nominal Starting Compositions, Annealing Treatments, and Long-Range Order Parameters (S)

Nominal Composition	Specimen No.	Annealing and Sintering Temperature°C	Time	S
$Cr_{79}Pt_{21}$	1	1300 **	9 hours	0.90
	2	1200	3 days	1.00
Cr_3Ir	1	"as-cast" *		0.89
	2	"as-cast"		0.89
$Cr_{72}Os_{28}$	1	1400 **	8 hours	0.64
	2	1400	24 hours	0.66
Cr_3Rh	1	1200	3 days	0.83
V_3Au	1	"as-cast"		0.99
	2	"as-cast" *		0.92
V_3Pt	1	"as-cast" *		0.95
	2	"as-cast"		0.98
V_3Ir	1	"as-cast"		0.94
V_3Rh	1	1200	3 days	
		1100	2 weeks	0.96
Ti_3Au	1	"as-cast"		0.97
Ti_3Pt	1	"as-cast" *		0.97
	2	"as-cast"		0.99
Ti_3Ir	1	"as-cast"		1.00
	2	"as-cast" *		0.91
Mo_4Pt	1	1600 **	48 hours	0.98
Mo_3Ir	1	1800	2 days	0.87
Mo_3Os	1	2000	2 days	0.81
Nb_3Au	1	"as-cast"		0.89
Nb_3Pt	1	1600	5 days	0.93
$Cr_{72}Ru_{28}$	1	800	6 weeks	0.55
V_3Pd	1	800	1 month	0.69

Table 3 (Cont)

Nominal Composition	Specimen No.	Annealing and Sintering Temperature °C	Time	S
Nb_3Os	1	1800	2 days	
		1600	5 days	0.90
Nb_3Ir	1	2000	3 hours	0.95

Note: All arc-melted alloy specimens were given a final annealing at 800 C for one hour followed by slow cooling except those marked (*) which were allowed to remain in the "as-cast" condition following arc-melting and solidification in a water-cooled copper hearth. Alloy specimens prepared by powder metallurgy were cooled from their sintering temperatures by turning off the furnace power. These are marked (**) and were not given a final anneal at 800 C.

All of the arc-melted alloys were given a final annealing at 800 C for one hour, followed by slow cooling to room temperature, except for Ti-Pt No. 1, Ti-Ir No. 2, V-Pt No. 1, V-Au No. 2, and Cr-Ir No. 1 (all marked with an asterisk in Table 3) which were examined in the "as-cast" condition. The powder metallurgy alloys were furnace-cooled from their sintering temperature to room temperature, in vacuo, by turning off the furnace power.

After the annealing treatments, the alloys were crushed in a hardened-steel rod mill to a 20-50 micron particle size. This size range was selected because it was ideal with respect to the avoidance of X-ray diffraction-line broadening on the one hand and preferred orientation on the other hand. The samples were not reannealed after crushing, since their X-ray patterns were devoid of any characteristic line broadening due to residual stresses. Spectrographic analyses of all powdered alloy samples revealed no major contaminants or impurities.

X-ray Diffraction

A Debye-Sherrer X-ray pattern was taken of each specimen for use in phase identification, indexing, detection of possible line broadening, and to assist in establishing the relative line intensities when extremely weak lines or possible preferred orientation effects might reduce the reliability of the diffractometer data. These patterns were given a standard eight-hour exposure at a constant tube current and voltage to facilitate comparison of relative intensities between films. A back-reflection focusing camera was used for precision lattice parameter determination. In addition, diffractometer data, were obtained for each specimen using an internal standard of either silver (a_o = 4.08625Å) or tungsten (a_o = 3.16504Å) powders. Lattice parameters were obtained by a least squares fitting of these data with greater weighting assigned to lines occurring at high Bragg angles. No angular extrapolation was used since the use of an internal standard appeared to compensate for the normal errors. The lattice parameters obtained are listed in Table 4.

The degree of long-range order (LRO) in each example was studied by using data obtained with nickel-filtered copper radiation on a General Electric XRD-3 Diffractometer. The -325 mesh alloy powder was carefully packed with an uniform standardized pressure into a tray which has a 24mm diameter and a 1.3mm deep depression. This size tray offered a maximum radiated area for a 1 degree tube slit, and its depth was selected so that the specimen could be considered to be of "infinite thickness." Special care was taken during specimen packing not to scrape or drag the surface, since this might result in preferred orientation effects on the observed relative intensities. The tray into which the sample was packed was attached to a small synchronous motor. The specimen was rotated by this motor about an axis normal to the specimen surface throughout the entire data-taking period in order to minimize any effect of preferred orientation.

Table 4

Lattice Parameters for Alloys Studied

Alloy, Number		a_o (in Angstroms)
Ti_3Ir	1	5.0082
	2	5.0087
Ti_3Pt	1	5.0309
	2	5.0327
Ti_3Au	1	5.0974
V_3Rh	1	4.7852
V_3Ir	1	4.7876
V_3Pt	1	4.8166
	2	4.8166
V_3Au	1	4.8813
	2	4.8807
Cr_3Rh	1	4.6731
$Cr_{72}Os_{28}$	1	4.6799
	2	4.6842
Cr_3Ir	1	4.6808
	2	4.6810
$Cr_{79}Pt_{21}$	1	4.6997
	2	4.7058
Nb_3Os	1	5.1348
Nb_3Ir	1	5.1333
Nb_3Pt	1	5.1524
Nb_3Au	1	5.2024
Mo_3Os	1	4.9689
Mo_3Ir	1	4.9682
Mo_4Pt	1	4.9878
$Cr_{72}Ru_{28}$	1	4.6765
V_3Pd	1	4.8254

Early results showed that the preferred orientation problem may be a serious one, as has also been noted by Courtney, Pearsall, and Wulff,(1965b). However, it appears that there is at least one unmistakable check that can be made for preferred orientation effects on all patterns. If one examines the LRO parameter contribution to the intensities for the (200) and the (211) reflections in Table 5, it can be seen that they are identical. A comparison of the ratio of these two peaks (See Figure 1) should then offer a good check on preferred orientation effects, since this ratio should be independent of the amount of LRO in the sample. If the (211) peak is normalized to a value of 1000, the (200) peak should in all cases have a value of about 460 if there is no preferred orientation present. The value of this observed intensity ratio was therefore used as a check for preferred orientation effects. A variation of greater than $\pm$10 percent was considered unacceptable, and any sample showing this much variation was repacked in the diffractometer specimen holder until satisfactory agreement was obtained.

Two diffractometer scans were taken of each specimen. One of these, at a chart speed of two degrees per minute, was used for indexing purposes and to ascertain the best proportional counter rate setting to obtain a maximum (211) count. The other scan, taken at a chart speed of 0.2 degrees per minute, was used for the integrated-peak-intensity data. All scans were made after an electronic warm-up period of at least one hour. Usually, the X-ray diffractometer data included 23 peaks. However, on a few samples, the highest angle peaks could not be traced because of the extremely high Bragg angles involved. In all cases, the patterns were indexed completely with all peaks accountable. In no instances were lines observed which would correspond to the (100) or (111) peaks; thus confirming the space group type: $Pm\bar{3}n$. The integrated intensity of each peak on the slow diffractometer trace was measured three times with a planimeter.

Table 5

LRO Parameter Contribution to A-15 Structure Factors

hkl	S Contribution to F
110	$2S(f_B-f_A)$
200	$S(f_B-f_A) + (3f_A+f_B)$
210	$S(f_B-f_A) - (3f_A+f_B)$
211	$S(f_B-f_A) + (3f_A+f_B)$
220	$2S(f_B-f_A)$
310	$2S(f_B-f_A)$
222	$3S(f_B-f_A) - (3f_A+f_B)$
320	$S(f_A-f_B) + (3f_A+f_B)$
321	$S(f_B-f_A) + (3f_A+f_B)$
400	$2(3f_A+f_B)$
411, 330	$2S(f_B-f_A)$
420	$S(f_B-f_A) + (3f_A+f_B)$
421	$(S-1)(f_B-f_A)-4f_A$
332	$S(f_B-f_A) + (3f_A+f_B)$
422	$2S(f_B-f_A)$
510, 431	$2S(f_B-f_A)$
520, 432	$S(f_A-f_B) + (3f_A+f_B)$
521	$S(f_B-f_A) + (3f_A+f_B)$
440	$2(3f_A+f_B)$
530, 433	$2S(f_B-f_A)$
600, 442	$S(f_B-f_A) + (3f_A+f_B)$
610	$S(f_B-f_A) - (3f_A+f_B)$
611, 532	$S(f_B-f_A) + (3f_A+f_B)$

The average of these three values, which seldom deviated by more than ±3 percent, was taken as the integrated intensity of the particular peak. A few of the specimens were found to have some extremely weak extraneous peaks, none of which superimposed on the basic A15 pattern. These were identified as resulting from small quantities of a second phase. Also, in some cases the beta component of the (211) peaks slightly overlapped the (210) peak. However, this contribution to the (210) peak could be easily subtracted. The value to be subtracted from the (210) intensity was obtained by measuring beta components of the (211) peak in several patterns where adequate resolution from the (210) peak was obtained. This percentage (4 percent) of the (211) peak was then subtracted from the (210) peak whenever an overlap was indicated. Aside from the above-mentioned weak peaks, the diffractometer traces were normal in all respects. In particular there were no indications of residual strains, abnormal line broadening, splitting of lines at high angles, or forbidden reflections. All peaks were very close to the usual Gaussian shape and could be readily indexed as resulting from the cubic A15-type structure. Typical X-ray patterns for a highly ordered and a partially disordered A15-type phase appear in Figure 1.

In the usual intensity equation for X-ray diffraction there are several terms which are angular dependent. To offset these factors and to minimize the effects of any long-time electronic circuitry effects, the ratios of adjacent integrated peak intensities were used as raw data for the determination of the long-range order parameters.

Model Calculations

A computer program was devised to assimilate the data in such a manner as to select the best ordering model to fit the data. This program contained atomic scattering factors obtained from the International Tables for X-ray Crystallography, (1962). Anomalous dispersion corrections were applied for all

of the elements studied based on the values given by Cromer, (1965). The usual analytical expression for the Lorentz polarization factors and multiplicity factors were used in the intensity calculations. A provision was also contained in the program to accommodate off-stoichiometric model calculations. This was done by inserting a chemical composition factor in the intensity equation (See Appendix A). Such a procedure is probably valid for small deviations (a few percent) from the "ideal" (A_3B) stoichiometric composition.

The observed data were compared first with ten different calculated models having long-range order parameters (S) from 0.0 (complete disorder) to 1.0 (complete order) in 0.1 increments (See Appendix A). When the region of maximum interest was found, the computer then compared the observed data with 20 other calculated models at 0.01 increments of S. The basis by which the computer selected the best ordering parameter was a minimization of the reliability factor:

$$R = \frac{1}{\Sigma W_i} \sum_{i=1}^{i=N} W_i \frac{(R_{oi} - R_{ci})^2}{R_{oi}\, R_{ci}} \qquad (1)$$

where

R is the reliability factor for a given S-value

N is the number of observed intensity ratios

R_o the observed intensity ratio

R_c the calculated intensity ratio

W_i is a weighting factor which was chosen as 10^4 for the (200)/(100), (210)/(200) and (211)/(210) intensity ratios; all other intensity ratios received weights of either five (ratios from (220)/(211) to (332)/(421)) or one (ratios beyond (332)/(421)).

After the best-fit model was selected, the calculated intentsities were normalized on the basis of a value of 1000 for the (211) peak. These calculated normalized values could then be compared directly with the observed normalized values.

The computer program contained two implicit assumptions which were further checked by experimental methods. The first assumption was that the models used need not consider the existence of lattice vacancies. This is particularly critical for the nonstoichiometric alloys. In these cases, it may be argued that the occurrence of the A15-type phase at a composition other than A_3B may be attributable to vacancies. However, in the chromium-osmium alloy the presence of lattice vacancies in an amount sifficient to produce the observed relative intensities would be easily detectable by means of a density measurement. The density value obtained in this case (Waterstrat and van Reuth, 1966) was much too high to permit the consideration of lattice vacancies as a major contribution to the intensity calculations. Density measurements on some of the other specimens led to similar conclusions.

The second assumption implicit in the computer program was that the diffractometer sensitivity on all peaks was the same. It became quite obvious in the course of this work, however, that the diffractometer was not detecting certain peaks which were extremely weak. These peaks were detected in the standardized Debye-Scherrer films but were undetected by the diffractometer. Values of the integrated intensities for such weak peaks were therefore assigned by means of a visual estimation of line intensities on the film. In all of these instances care was taken that the correspondence between the film peaks and the diffractometer peaks was qualitatively consistent on all peaks.

EXPERIMENTAL RESULTS

The results of this study on the degree of long-range order in 20 samples exhibiting the A15 structure appear in Table 6. Below each alloy designation there are four columns of intensity values. The first column lists the observed relative intensities of all lines in the Debye-Sherrer films. The second column contains the intensity values observed from the planimetered diffractometer traces. The values shown in column three for each specimen are those calculated by the computer for the selected model whose S-value appears at the head of that column. The fourth column lists the intensity values one would expect for a completely ordered structure (S = 1.0). (When the computer selected an LRO parameter of 1.0, column three has been so labelled and column four omitted.) In general, it can be seen that the titanium and vanadium alloys are nearly completely ordered. However, when chromium is the A-element, there appears a rather wide variance in the degree of LRO. A trend is obvious for the chromium alloys in which osmium, iridium and platinum are the B-elements. Of these three, the osmium alloy has the lowest degree of ordering, the platinum alloy has the highest degree of order, and the iridium alloy has an intermediate value. In this series, then, it appears that, as the B-element is selected from a column closer to the manganese column in the periodic table, the degree of ordering decreases. The same correlation appears to hold where molybdenum is the A-element. In this case, the osmium alloy again exhibits the lowest degree of order. It is alwo worthy of note that most of the molybdenum alloys are more disordered than the corresponding alloys containing niobium. These relationships are summarized in Figure 2.

Table 6 contains calculated intensities for two different compositions in the Mo-Pt system. A binary A15-type phase has been reported in this system at the composition Mo_{85} Pt_{15} by Sadogopan, Gatos, and Giessen, (1965); using arc-melted alloys.

Table 6

Comparison of Observed and Calculated Intensities

For Samples Annealed at 800 C

Cr_3Rh

hkl	Relative Intensities Observed Film	Observed Diff.	Calculated S = 0.83	Calculated S = 1.00
110	MW	165	165	226
200	MS	467	469	468
210	S^+	743	712	624
211	VS	1000	1000	1000
220	VW	27	24	33
310	W	35	34	46
222	VW	-	19	11
320	MS	138	136	118
321	S	488	475	477
400	MS	144	142	134
411, 330	-	18	23	31
420	MS	125	151	152
421	MS	117	141	122
332	MS	113	142	143
422	-	-	13	18
510, 431	W	36	42	57
520, 432	MS	234	231	198
521	S	351	346	349
440	MS	246	292	277
530, 433	W	-	54	74
600, 442	S^+	-	654	659
			R = 0.0248	R = 0.0694

MW = medium weak
MS = medium strong
VW = very weak
VS = very strong
W = weak
M = medium
S = strong
(+) or (-) modifies indicated value by plus or minus
Diff = diffractometer

Table 6 (Cont.)

$Cr_{7.9}Pt_{21}$					Cr_3Ir				
	Relative Intensities					Relative Intensities			
	Observed		Calculated			Observed		Calculated	
hkl	Film	Diff.	S = 1.00		hkl	Film	Diff.	S = 0.89	S = 1.00
110	MS^+	565	575		110	MS^+	538	510	606
200	MS	476	458		200	MS	453	458	457
210	M	315	307		210	M	368	349	291
211	VS	1000	1000		211	VS	1000	1000	1000
220	MW	109	89		220	MW	102	78	93
310	M	121	126		310	M	113	112	133
222	_	_	<1		222	-	-	<1	1
320	MW	69	58		320	MW	64	67	55
321	S	484	503		321	S	475	503	505
400	M	133	108		400	M	116	113	107
411, 330	M^-	113	83		411, 330	M^-	72	75	87
420	MS	161	160		420	MS	178	161	162
421	MW	55	59		421	MW	55	69	57
332	MS	117	151		332	MS	123	152	153
422	MW	51	47		422	MW^-	47	42	50
510, 431	MS	120	145		510, 431	MS	136	130	154
520, 432	MW	65	94		520, 432	MW	81	113	92
521	S	290	356		521	S	340	364	366
440	MS	210	213		440	MS	144	231	218
530, 433	M	125	172		530, 433	M	85	162	190
600, 442	S^+	-	548		600, 442	S^+	382	635	635
		R = 0.0063					R = 0.0045		R = 0.0439

Table 6 (Cont.)

$Cr_{72}Os_{28}$

hkl	Relative Intensities Observed Film	Diff.	Calculated S = 0.66	S = 1.00
110	M	281	309	519
200	MS	464	459	458
210	MS	471	511	341
211	VS	1000	1000	1000
220	W	45	48	81
310	MW	71	68	115
222	-	-	4	<1
320	M	98	100	64
321	S	509	499	503
400	M+	135	130	112
411, 330	MW	45	45	76
420	MS	155	159	160
421	M	97	105	66
332	MS	157	149	151
422	W	-	24	43
510, 431	M	90	78	133
520, 432	MS	174	171	107
521	S+	342	357	360
440	MS+	245	264	224
530, 433	M	93	96	192
600, 442	S+	612	622	609

R = 0.0206 R = 0.2036

V_3Pd

hkl	Relative Intensities Observed Film	Diff.	Calculated S = 0.69	S = 1.00
110	MW	154	153	286
200	MS	466	465	465
210	S	715	707	528
211	VS	1000	1000	1000
220	W	28	23	44
310	MW	38	32	60
222	VW	18	20	6
320	MS	137	139	103
321	S	503	467	468
400	MS	152	139	123
411, 330	W	23	18	33
420	MS	123	137	137
421	MS	110	137	102
332	MS	120	124	124
422	VW	-	9	16
510, 431	MW	50	26	48
520, 432	MS+	159	195	147
521	S	212	255	255
440	MS+	179	211	187
530, 433	W	20	24	44
600, 442	S	254	262	261
610	MW	-	136	102
611, 532	VS	-	1024	1021

R = 0.0007 R = 0.1952

Table 6 (Cont.)

$Cr_{72}Ru_{28}$

hkl	Relative Intensities Observed Film	Diff.	Calculated S = 0.55	S = 1.00
110	VW	61	66	188
200	MS	435	471	470
210	VS	935	908	657
211	VS	1000	1000	1000
220	-	-	10	29
310	VW	20	14	39
222	W	44	40	15
320	MS	130	173	124
321	S	466	456	458
400	MS	122	152	132
411, 330	-	-	8	22
420	MS	132	138	138
421	MS	140	177	128
332	MS	132	128	128
422	-	-	4	12
510, 431	VS	14	12	36
520, 432	MS+	248	287	207
521	S	278	301	301
440	MS+	242	293	254
530, 433	VS	-	14	42
600, 442	S+		515	515
			R = 0.0086	R = 0.5092

V_3Rh

hkl	Relative Intensities Observed Film	Diff.	Calculated S = 0.96	S = 1.00
110	M	262	253	270
200	MS	456	465	464
210	S	635	587	567
211	VS	1000	1000	1000
220	W	48	36	39
310	MW	55	51	55
222	-	-	9	8
320	MS	117	114	110
321	S	442	481	481
400	MS	138	132	130
411, 330	W	28	33	35
420	MS-	159	149	148
421	MS-	111	115	110
332	MS	131	156	137
442	VW	-	18	19
510, 431	MW	69	58	58
520, 432	MS	159	174	164
521	S	221	309	301
440	MS+	172	232	221
530, 433	W	41	30	62
600, 442	S	276	371	344
610	MW	149	156	133
611, 532	VS	-	2509	-
			R = 0.0199	R = 0.0221

Table 6 (Cont.)

V_3Au					V_3Pt				
	Relative Intensities					Relative Intensities			
	Observed		Calculated			Observed		Calculated	
hkl	Film	Diff.	S = 0.99	S = 1.00	hkl	Film	Diff.	S = 0.98	S = 1.00
110	S	640	616	625	110	S	679	654	673
200	MS	463	453	453	200	MS	467	454	454
210	M	284	278	273	210	M	266	262	253
211	VS	1000	1000	1000	211	VS	1000	1000	1000
220	MW	113	97	98	220	MW	108	101	104
310	M	149	139	140	310	M	144	143	147
222	-	-	2	2	222	-	9	2	3
320	MW$^-$	44	54	53	320	MW$^-$	47	51	49
321	S	488	506	506	321	S	543	507	508
400	M	98	105	104	400	M	150	104	103
411, 330	M$^-$	78	87	89	411, 330	M$^-$	97	90	93
420	M$^+$	128	154	154	420	M$^+$	178	157	157
421	MW	48	51	50	421	MW	54	51	49
332	M$^+$	114	141	141	332	M$^+$	151	145	145
422	MW	54	46	47	422	MW	54	49	50
510, 431	M$^+$	122	138	140	510, 431	M$^+$	180	147	151
520, 432	MW	64	70	69	520, 432	MW	72	74	71
521	MS	280	287	287	521	MS	278	309	310
440	M$^+$	151	155	155	440	M	144	170	167
530, 433	M	121	126	128	530, 433	M	122	144	148
600, 442	MS	280	274	274	600, 442	MS	300	328	329
610	W	-	42	41	610	W	43	53	51
611, 532	VS	-	943	924	611, 532	VS	1312	1335	1341
			R = 0.0004	R = 0.0007				R = 0.0007	R = 0.0015

Table 6 (Cont.)

	V_3Ir				Ti_3Au				
	Relative Intensities					Relative Intensities			
	Observed		Calculated			Observed		Calculated	
hkl	Film	Diff.	S = 0.94	S = 1.00	hkl	Film	Diff.	S = 0.97	S = 1.00
110	S	658	600	656	110	S	709	684	715
200	MS	464	454	454	200	MS	440	448	448
210	M	306	291	261	210	M	250	236	222
211	VS	1000	1000	1000	211	VS	1000	1000	1000
220	MW	119	93	101	220	MW	128	110	115
310	M	166	131	144	310	M	188	156	163
222	-	-	1	3	222	-	-	4	5
320	MW$^-$	60	57	51	320	MW	56	47	44
321	S	548	508	509	321	S	516	514	515
400	M	106	108	104	400	M	105	101	99
411, 330	M	118	84	92	411, 330	M	114	96	99
420	M$^+$	164	158	159	420	M$^+$	143	151	151
421	MW	51	57	51	421	MW	41	44	41
332	M$^+$	153	147	147	332	M$^+$	136	135	136
422	MW	58	46	50	422	MW	50	47	49
510, 431	M$^+$	161	138	151	510, 431	M$^+$	155	135	141
520, 432	MW	92	85	75	520, 432	MW	39	53	50
521	MS	336	320	320	521	MS	230	240	240
440	M	200	184	178	440	M$^+$	103	120	118
530, 433	M	117	140	152	530, 433	M	95	102	106
600, 442	MS	330	360	361	600, 442	MS	172	186	186
610	W	49	69	61	610	W	23	24	22
611, 532	VS	1490	1808	1812	611, 532	VS	486	518	517
			R = 0.0040	R = 0.0148				R = 0.0046	R = 0.0117

Table 6 (Cont.)

	Ti_3Pt				Ti_3Ir			
	Relative Intensities				Relative Intensities			
	Observed		Calculated		Observed		Calculated	
hkl	Film	Diff.	S = 0.99	S = 1.00	hkl	Film	Diff.	S = 1.00
110	S	698	694	704	110	S	652	688
200	MS	458	449	449	200	MS	444	449
210	M	238	234	230	210	M	224	238
211	VS	1000	1000	1000	211	VS	1000	1000
220	MW	120	110	111	220	MW	108	109
310	M	165	157	159	310	M	172	155
222	-	-	5	4	222	-	-	4
320	MW	56	47	46	320	MW	52	47
321	S	522	512	512	321	S	509	513
400	M	91	101	100	400	M	103	101
411, 330	M	87	96	98	411, 330	M	116	96
420	M^+	134	152	152	420	M^+	130	153
421	MW	40	44	43	421	MW	23	44
332	M^+	123	137	137	332	M^+	121	138
422	MW	50	48	49	422	MW	58	48
510, 431	M^+	134	140	141	510, 431	M^+	121	140
520, 432	MW	59	55	54	520, 432	MW	42	57
521	MS	228	252	251	521	MS	229	256
440	M^+	120	127	126	440	M^+	112	131
530, 433	M	120	110	110	530, 433	M	121	102
600, 442	MS	191	205	205	600, 442	MS	198	212
610	W	30	26	26	610	W	30	28
611, 532	VS	392	591	589	611, 532	VS	406	621
			R = 0.0008	R = 0.0014				R = 0.0033

Table 6 (Cont.)

	Nb_3Au				Nb_3Pt			
	Relative Intensities				Relative Intensities			
	Observed		Calculated		Observed		Calculated	
hkl	Film	Diff.	S = 0.89	S = 1.00	hkl	Film	Diff.	S = 0.93	S = 1.00
110	M	193	185	225	110	M	189	188	213
200	MS	452	444	444	200	MS	429	445	445
210	S	630	633	578	210	S	610	630	595
211	VS	1000	1000	1000	211	VS	1000	1000	1000
220	W	27	31	37	220	W	44	31	35
310	MW	41	44	53	310	MW	54	44	50
222	VW	-	16	11	222	VW	33	15	12
320	MS	140	139	127	320	MS	163	138	130
321	VS	502	523	523	321	VS	538	521	522
400	MS	149	150	144	400	MS	140	149	145
411, 330	W	18	27	32	411, 330	W	25	27	30
420	MS$^+$	138	152	153	420	MS$^+$	171	153	153
421	MS	125	134	122	421	MS	150	134	126
332	MS	102	136	136	332	MS	102	137	137
422	VW	-	12	15	422	VW	13	13	14
510, 431	MW	16	36	43	510, 431	MW	38	36	41
520, 432	MS	109	160	145	520, 432	MS	163	163	154
521	S	188	229	235	521	S	214	235	236
440	MS	133	167	160	440	MS	142	172	169
530, 433	VW	-	24	30	530, 433	VW	38	26	30
600, 442	MS	130	167	167	600, 442	MS	135	176	177
610	MW	50	65	60	610	MW	58	72	66
611, 532	S	358	447	448	611, 532	S	388	479	481
			R = 0.0138	R = 0.0338				R = 0.0018	R = 0.0082

Table 6 (Cont.)

Nb_3Ir					Nb_3Os				
	Relative Intensities					Relative Intensities			
	Observed		Calculated			Observed		Calculated	
hkl	Film	Diff.	S = 0.95	S = 1.00	hkl	Film	Diff.	S = 0.90	S = 1.00
110	M	189	184	200	110	M	175	157	188
200	MS	468	446	445	200	MS	442	446	445
210	S	620	638	614	210	S	730	680	631
211	VS	1000	1000	1000	211	VS	1000	1000	1000
220	W	41	30	33	220	W	40	26	31
310	MW	52	43	47	310	MW	57	37	45
222	VW	23	16	14	222	VW+	21	20	15
320	MS	152	139	134	320	MS	142	148	138
321	VS	512	522	522	321	VS	500	521	522
400	MS	132	150	147	400	MS	149	153	149
411, 330	W	32	27	29	411, 330	W	43	23	27
420	MS+	139	153	154	420	MS+	135	153	153
421	MS	127	136	130	421	MS	127	145	134
332	MS	132	137	138	332	MS	104	137	137
422	VW	12	13	14	422	VW	7	11	13
510, 431	MW	52	36	39	510, 431	MW	28	31	36
520, 432	MS	155	172	161	520, 432	MS	130	180	165
521	S	220	239	240	521	S	213	239	238
440	MS	141	172	174	440	MS	135	182	175
530, 433	VW	30	26	28	530, 433	VW	10	22	26
600, 442	MS	164	186	181	600, 442	MS	151	181	180
610	MW	73	73	70	610	MW	66	79	72
611, 532	S	416	496	498	611, 532	S	382	501	492
			R = 0.0009	R = 0.0045				R = 0.0090	R = 0.0245

Table 6 (Cont.)

	Mo_xPt_y				Mo_3Ir				
	Relative Intensities					Relative Intensities			
	Observed		Calculated			Observed		Calculated	
hkl	Film	Diff.	S = 0.98 $Mo_{80}Pt_{20}$	S = 0.98 $Mo_{85}Pt_{15}$	hkl	Film	Diff.	S = 0.87	S = 1.00
110	M	144	138	86	110	M	158	146	185
200	MS	452	450	450	200	MS	442	449	449
210	S^+	810	714	820	210	S^-	742	704	641
211	VS	1000	1000	1000	211	VS	1000	1000	1000
220	W	18	23	15	220	W	21	24	30
310	MW	35	33	21	310	MW	30	34	43
222	W	17	23	35	222	W	16	22	16
320	MS	174	154	176	320	MS	177	152	138
321	VS	500	516	515	321	VS	545	517	517
400	MS	170	155	164	400	MS	140	155	149
411, 330	W	13	20	13	411, 330	W	21	21	27
420	MS	139	155	155	420	MS	140	156	156
421	MS	130	154	177	421	MS	130	153	139
332	MS^-	110	141	141	332	MS^-	126	142	142
422	VW	-	12	7	422	W	-	11	13
510, 431	MW	18	30	19	510, 431	MW	22	30	39
520, 432	MS	217	207	237	520, 432	MS	153	207	189
521	S	248	267	267	521	S	251	271	273
440	MS	152	212	225	440	MS	140	215	208
530, 433	W	-	31	16	530, 433	W	-	24	32
600, 442	MS	165	226	226	600, 442	MS	153	233	235
610	M	104	105	121	610	M	93	108	99
611, 532	VS	615	671	671	611, 532	VS	567	699	708
			R = 0.0107	R = 0.0887				R = 0.0117	R = 0.0360

Table 6 (Cont.)

Mo_3Os

hkl	Relative Intensities Observed Film	Diff.	Calculated S = 0.81	S = 1.00
110	M	125	120	173
200	MS	497	450	449
210	S	734	752	659
211	VS	1000	1000	1000
220	W	21	20	28
310	MW	30	28	40
222	MW	20	27	17
320	MS	166	162	141
321	VS	507	516	517
400	MS	169	159	150
411, 330	MW	22	18	25
420	MS	160	155	156
421	MS	156	164	143
332	MS	127	141	142
422	VW	-	9	12
510, 431	MW	20	25	36
520, 432	MS	190	222	194
521	S	211	271	271
440	MS	177	222	210
530, 433	W	10	20	28
600, 442	MS	170	234	234
610	M	97	117	102
611, 532	VS	557	704	705
			R = 0.0066	R = 0.0655

We have prepared alloys at this compositon by both arc-melting and power metallurgy methods, but the X-ray patterns of these alloys contained Mo lines. Consequently, we repeated our alloy preparation method on an arc-melted sample and on a powder sample both having the nominal composition Mo_4Pt and this time the X-ray patterns did not contain Mo lines. The X-ray patterns of the alloys Mo_4Pt did contain a few very weak lines in addition to the lines of an A15-type phase and it is possible that this alloy has not been annealed long enough to permit a complete reaction. Lines of the A15-type phase were very sharp and prominent, however, even at high angles where an excellent resolution of the Kα doublet was observed. The line intensities of the A15-type phase in this alloy were therefore measured with the diffractometer and compared with calculated intensities for both the $Mo_{85}Pt_{15}$ and the Mo_4Pt compositions.

The order parameters obtained for the Mo-Pt A15 phase were between 0.96 and 1.00 depending on the weighting of the lines and on the assumed composition.

Neither of the two assumed compositions permit a completely satisfactory agreement between observed and calculated intensities as can be seen in Table 6. It appears, however, that a satisfactory agreement might be obtained for a composition lying somewhere between the two assumed compositions and further work would be required in order to verify the exact composition of this phase. Nevertheless, it appears safe to conclude that the order parameter for the Mo-Pt A15-type phase is approximately 0.98 within the limits of experimental error ($\pm$0.05).

In the Cr_3Ir, Ti_3Ir, Ti_3Pt, and V_3Au systems, additional samples were made in precisely the same manner except for the final annealing at 800 C. These new specimens were prepared in order to permit a comparison of the LRO

parameters in specimens which had been subjected to fast cooling in contrast to specimens which had been slowly cooled from lower temperatures.

In two of these samples (Ti_3Ir and V_3Au), when the degree of order was restudied, it was found to differ slightly from the previous values, as shown in Table 3. An error analysis of our data leads us to believe that our LRO parameters for alloys containing Cr, V, or Ti, are accurate to a value of ± 0.03 and alloys containing Mo of Nb to about ± 0.05. Therefore, the above-mentioned changes in the degree of order with heat treatment appear to be significant. In addition, these samples exhibited differing superconducting transition temperatures which will be reported in a future publication (Blaugher, Hein, Cox, van Reuth, and Waterstrat, 1967). These results suggest a possible relationship between the LRO parameter (S) and the superconducting transition temperature (T_c) in A15-type phases.

Examination of the observed and calculated intensities given in Table 6 reveals that in many cases the observed intensities of peaks occurring at the higher Bragg angles are considerably weaker than the calculated values. These diminished intensities may result from the effect of a temperature factor. In order to test this hypothesis, several of the more intense peaks occurring at the highest Bragg angles in each pattern were measured in the diffractometer at both room temperature and at liquid nitrogen temperature. In each case where the room temperature data suggested a temperature factor contribution to the intensities, an enhancement of the observed intensities was found to occur at the liquid nitrogen temperature. The increased intensity at liquid nitrogen temperature seemed, in all cases, adequate to explain the high-angle intensity discrepancies at room temperature as being largely due to the influence of a temperature factor. It may be noteworthy that the temperature factor correction appears to be unusually small in the A15-type phases containing Ti or V as the A-element and also when the A-atom positions have mixed occupancy.

DISCUSSION

In the course of this investigation of the A15 structures, two of these phases were found to occur at compositions other than the ideal A_3B. These have been reported elsewhere (Waterstrat and van Reuth, 1966). In addition to these, a vanadium-osmium A15-type phase, occurring approximately at the equiatomic composition, has been discovered recently by Raub and Röschel, (1966). These findings coupled with the previously reported off-stoichiometric A15-type phases (Darby and Zegler, 1962; Nevitt, 1962; Hartley, Parsons, and Seedly, 1964; Ray and Parsons, 1966; Sadogopan, Gatos, and Giessen, 1965) add considerable impetus to questions of fundamental importance. Since this structure occurs so frequently, it obviously has a rather high degree of stability. Because many of these phases do not even include the ideal A_3B composition, stoichiometry cannot be weighed too heavily in stability considerations. In fact, since the A_3B composition is not even included in some instances, some of the A-atoms are forced to occupy B-positions and vice versa. Therefore, one must search for other factors leading to the stability of the A15 structure. One such factor appears to be related to a generalized plot first shown by Nevitt, (1962).

Figure 3 is a plot similar to Nevitt's except that we have utilized the lattice parameter data obtained in the present investigation. It now appears that points obtained for A15-type phases having a common A-element (Ti, V, Cr, Nb, Mo) fall along separate straight lines having similar slopes but different extrapolated origins. Thus, the observed "contractions" in the direction of the A-A interatomic distances depend not only on the Goldschmidt radius ratios (R_A/R_B) but also on the identity of the A-element. Of particular interest in this connection is the "contraction" occurring when the Goldschmidt radius of the A-element and the B-element are identical ($R_A/R_B = 1$). In this

special case, the observed A-A interatomic distances for each A-element relative to the distances observed in each pure element may be compared. Assuming a value of unity for the CN12 interatomic distance in the pure elements, one obtains the following values for the A-A interatomic distances in the corresponding A15-type phases (at $R_A/R_B = 1$): Ti 0.875 V 0.889 Cr 0.889 Nb 0.892 Mo 0.894. Thus it appears that sizable contractions occur in the direction of the A-A interatomic distances even when the Goldschmidt radii of the A- and B-elements are identical.

The existence of these abnormally short distances between atoms in the A-positions is suggestive of a strong electronic bonding (Nevitt, 1962). However, Frank and Kasper, (1958); have pointed out that packing considerations alone would suffice to account for this behavior as well as for similar effects occurring in the sigma phases. It may be noted that for simultaneous A-A and A-B atom contacts in the A15-type structure, assuming the atoms are spherical, the radius of the A-atom would be 0.81 relative to a value of unity for the B-atom, (Nevitt, 1962). The A-A interatomic distances observed would, therefore, be compatible with this hard sphere model only if the radii of the B-atoms were slightly greater than the Goldschmidt radius values. It appears that the radius of the A-atoms can undergo variable contractions, depending on the value of the effective atomic radius for its B-atom partner. This would account for the observed variations in the contraction of the A-A interatomic distances shown in Figure 3.

In view of these realtionships it seems highly probable that phase stability would depend not only on the relative sizes of the atoms as expressed by the Goldschmidt radius ratios, with their implicit assumption of rigid, spherical atoms, but rather on the ability of the atoms to undergo sizable deformations. The degree of atomic ordering in the A15-type phases could

also be expected to depend on the ability of each constituent atom to undergo appreciable deformation. These deformations would accompany the interchange of atoms between two crystallographic lattice sites differing markedly in their coordination geometry.

Our results seem to indicate that elements such as Cr or Os possess a greater ability to undergo the required deformation than do atoms such as Ti or Pt. In fact, an increased tendency toward disorder is noted as one selects either A- or B-elements progressively closer to the manganese column in the periodic table (Figure 2). These periodic table effects may be an indication of an intimate relationship between the eletronic structure and the ability of the atoms to undergo size adjustments. Any gain in phase stability resulting from a more efficient atomic packing must certainly be balanced against possible gains or losses in stability resulting from concomitant changes in the electronic band structure.

It is also interesting to compare the data obtained on atomic ordering in these binary A15-type phases with similar data on atomic ordering in binary sigma phases (Kasper and Waterstrat, 1956; Wilson and Spooner, 1963; Forsyth and d'Alte da Veiga, 1963; Wilson, 1963; Spooner and Wilson, 1964; Algie and Hall, 1966). Both the sigma and the A15-type structures may be regarded as determined by geometrical requirements for sphere packing (Frank and Kasper, 1958, 1959). The atomic packing requirements seem to be partly responsible for the occurrence of common structural features in these phases. In particular, both structures contain chains of atoms with abnormally short interatomic distances. As shown in Figure 4 each atom in these chains occurs at the center of an atomic polyhedron formed by 14 near neighbors in which two planar atomic hexagons share a common hexagonal axis. These hexagons are

rotated with respect to each other. The atoms forming the chains are sandwiched between the hexagons and each atom chain coincides with a hexagonal axis.

The data on atomic ordering for both sigma and the A15-type phases (Tables 7 and 8) reveal that the atom chains are frequently preferred sites for atoms such as Ti, V, Cr, Mo, or Nb, but a mixed occupancy is also frequently observed (Table 7). Atoms to the right of the manganese column in the periodic table (B-elements) show a definite preference for atom sites having the icosahedral 12-fold coordination in both structures. Although these effects may be attributed to the operation of an "atomic-size"factor, it is important to consider the sphere-packing principles for these phases as described by Frank and Kasper, (1958, 1959). These principles require that the atoms in such structures should behave not as "rigid" spheres but with a considerable capacity for undergoing deformation. Thus, it would appear that the atomic ordering in these phases might depend largely on the ability of the constituent atoms to undergo the necessary deformation.

If the ability to undergo such deformation were related to electronic structures or to the position of the constituent atoms in the periodic table, then one might expect to observe common trends with respect to atomic ordering in both the sigma and A15-type phases. In this connection it is interesting to note that, among all binary sigma- and A15-type structures in which atomic ordering has been studied, the most considerable disorder has been observed in the chromium-osmium phases. Furthermore the chromium phases, in general, seem more disordered than do the vanadium or niobium phases. Phases containing molybdenum appear to be slightly more disordered than phases containing niobium, but perhaps not quite as highly disordered as the chromium phases.

Table 7

Order Parameters for Binary Sigma Phases and Fractional Occupancy of Each Atomic Site

System	Order Parameters*					Composition (Atomic %B)*	Fractional Occupancy, Percent				
	2(a) CN12	4(f) CN15	8(i) CN14	8(i) CN12	8(j) CN14		2(a) CN12	4(f) CN15	8(i) CN14	8(i) CN12	8(j) CN14
V-Ni	0.78+	0.92	0.80	0.80+	0.96	31 Ni	85.0 Ni	2.5 Ni	6.3 Ni	86.3 Ni	1.2 Ni
	0.84+	1.00	0.48	0.89+	0.97	36 Ni	90.0 Ni	0.0 Ni	18.7 Ni	91.3 Ni	1.2 Ni
	0.75+	1.00	0.23	0.80+	0.84	39 Ni	85.0 Ni	0.0 Ni	30.0 Ni	87.5 Ni	6.2 Ni
V-Fe	0.75+	1.00	0.53	0.75+	0.38	40 Fe	85.0 Fe	0.0 Fe	18.7 Fe	85.0 Fe	25.0 Fe
V-Mn	1.00+	0.32	0.21+	1.00+	0.18	81 Mn	100.0 Mn	55.0 Mn	85.0 Mn	100.0 Mn	66.2 Mn
Cr-Co	0.43+	0.87	0.62	0.39+	0.31+	39 Co	65.0 Co	5.0 Co	15.0 Co	62.5 Co	50.0 Co
Cr-Fe	0.35+	0.17	0.02+	0.24+	0.07	54 Fe	70.0 Fe	45.0 Fe	55.0 Fe	65.0 Fe	50.0 Fe
Cr-Mn	1.00+	0.00	0.17	1.00+	0.25	75 Mn	100.0 Mn	75.0 Mn	62.5 Mn	100.0 Mn	56.3 Mn
	0.50+	0.19	0.25+	0.75+	0.19	80 Mn	90.0 Mn	65.0 Mn	85.0 Mn	95.0 Mn	65.0 Mn
Cr-Re	0.58	0.38+	0.22+	0.17	0.06+	60 Re	25.0 Re	75.0 Re	68.8 Re	50.0 Re	62.5 Re
Nb-Ir	1.00+	1.00	0.69	1.00+	0.69	40 Ir	100.0 Ir	0.0 Ir	12.5 Ir	100.0 Ir	12.5 Ir
Nb-Os	1.00+	1.00	1.00	1.00+	0.38	40 Os	100.0 Os	0.0 Os	0.0 Os	100.0 Os	25.0 Os
Nb-Re	1.00+	1.00	0.26	1.00+	0.26	55 Re	100.0 Re	0.0 Re	40.6 Re	100.0 Re	40.6 Re
Mo-Ir	0.31+	1.00	1.00	0.74+	0.55	28 Ir	50.0 Ir	0.0 Ir	0.0 Ir	81.3 Ir	12.5 Ir
Mo-Re	1.00+	0.55	0.09	0.58+	0.32	55 Re	100.0 Re	25.0 Re	50.0 Re	81.2 Re	37.5 Re
	1.00+	0.25	0.25	1.00+	0.25	67 Re	100.0 Re	50.0 Re	50.0 Re	100.0 Re	50.0 Re
Mo-Os	0.62+	1.00	0.82	0.91+	0.64	35 Os	75.0 Os	0.0 Os	6.2 Os	93.8 Os	12.5 Os
Mo-Co	1.00+	1.00	0.69	1.00+	0.69	40 Co	100.0 Co	0.0 Co	12.5 Co	100.0 Co	12.5 Co
Mo-Fe	1.00+	0.50	0.50	1.00+	0.50	50 Fe	100.0 Fe	25.0 Fe	25.0 Fe	100.0 Fe	25.0 Fe
Mo- Mn	1.00+	1.00	0.00	1.00+	0.21	63 Mn	100.0 Mn	0.0 Mn	62.5 Mn	100.0 Mn	50.0 Mn

*Elements in the Mn column or to the right of the Mn column in the Periodic Table are designated as "B-elements." Elements to the left of the Mn column are designated as "A-elements." Order parameters are printed with plus sign (+) for atom sites preferred by "B-elements."

Table 8

Order Parameters for Binary A-15 Type Phases (Annealed at 800 C)
And Fractional Occupancy Of Each Atomic Site

System	Order Parameter* Atomic Site 6(c) CN14	2(a) CN12	Composition (Atomic %B)*	Fractional Occupancy, Percent Atomic Site 6(c) CN14	2(a) CN12
Ti-Au	0.97	0.97+	25 Au	0.7 Au	97.8 Au
Ti-Pt	0.99	0.99+	25 Pt	0.2 Pt	99.3 Pt
Ti-Ir	1.00	1.00+	25 Ir	0.1 Ir	100.0 Ir
V-Au	0.99	0.99+	25 Au	0.2 Au	99.3 Au
V-Pt	0.98	0.98+	25 Pt	0.5 Pt	98.5 Pt
V-Ir	0.94	0.94+	25 Ir	1.5 Ir	95.5 Ir
V-Rh	0.96	0.96+	25 Rh	1.0 Rh	97.0 Rh
V-Pd	0.69	0.69+	25 Pd	7.7 Pd	76.8 Pd
Cr-Pt	1.00	0.80+	21 Pt	0.0 Pt	84.0 Pt
Cr-Ir	0.89	0.89+	25 Ir	2.7 Ir	91.8 Ir
Cr-Os	0.57	0.66+	28 Os	12.2 Os	75.6 Os
Cr-Rh	0.83	0.83+	25 Rh	4.2 Rh	87.3 Rh
Cr-Ru	0.47	0.55+	28 Ru	14.8 Ru	67.6 Ru
Nb-Au	0.89	0.89+	25 Au	2.7 Au	91.8 Au
Nb-Pt	0.93	0.93+	25 Pt	1.7 Pt	94.8 Pt
Nb-Ir	0.95	0.95+	25 Ir	1.2 Ir	96.3 Ir
Nb-Os	0.90	0.90+	25 Os	2.5 Os	92.5 Os
Mo-Pt	0.98	0.74+	20 Pt	0.4 Pt	78.8 Pt
Mo-Ir	0.87	0.87+	25 Ir	3.2 Ir	90.3 Ir
Mo-Os	0.81	0.81+	25 Os	4.7 Os	85.8 Os

*Elements in the Mn column or to the right of the Mn column in the Periodic Table are designated as "B-elements." Elements to the left of the Mn column are designated as "A-elements." Order parameters are printed with plus sign (+) for atom sites preferred by "B-elements."

These observations suggest that consideration should be given to the effects of chemical composition on the atomic ordering and on phase stability in general. One may note that in alloy systems where both a sigma phase and an A-15 type phase co-exist, the sigma phase usually possesses a broader composition range of stability. Perhaps the sigma structure is more stable because of the smaller geometric distortions required for its formation (Frank and Kasper, 1959).

The periodic table relationships giving rise to "composition shifts" in both of these phase types (Sully, 1951-1952; Rideout, Manly, Kamen, Lement,

and Beck, 1951; Greenfield and Beck, 1954; Waterstrat and van Reuth, 1966) have been discussed as evidence of "electron compound" behavior. However, these "composition shifts" can also be explained by assuming that certain critical ranges of the "electron concentration" create favorable conditions for atom deformation. Thus, even if packing considerations are of major importance in stabilizing these phases, the formation of appropriate atom sizes may be facilitated within certain ranges of "electron concentration." The remarkable stability of the sigma- and A15-type phases would, therefore, result not primarily from the interaction of free electrons with the Brillouin zones as in the classical "electron compound" picture, but rather from the interdependence between electronic structure and the ability of the atoms to conform to geometrical packing requirements.

Although a quantitative evaluation of these relationships would be highly desirable, our present understanding of the electronic structure of the transition elements is incapable of dealing with this problem. Nevertheless, the qualitative relationships obtained experimentally in the present study may be helpful in understanding and perhaps even in predicting certain effects. One might estimate the probable degree of atomic ordering in a given alloy and possible deviations from the "ideal" stoichiometry. Such information may be helpful in evaluating certain physical properties, such as the superconducting transition temperature, when these properties are partially dependent on the nature and degree of atomic ordering.

ACKNOWLEDGMENTS

It is a pleasure to acknowledge the diligent efforts of Mr. J. H. Brady and Miss R. Usatchew of the U. S. Navy Marine Engineering Laboratory in the X-ray diffractometry. The precision lattice parameters in Table 4 were obtained by Mr. H. E. Swanson at the National Bureauof Standards

References

1 - Algie, S.H., and E.O. Hall (1966). Acta Cryst. 20 142

2 - Blaugher, R.D., R.A. Hein, J. Cox, E.C. van Reuth, and R.M. Waterstrat, (1967), To be published

3 - Cromer, D.T. (1965) Acta Cryst. 18 17

4 - Courtney, T.H., G.W. Pearsall, and J. Wulff, (1965a) Trans. AIME, 233, 212

5 - Courtney, T.H., G.W. Pearsall, and J. Wulff, (1965b) J. Appl. Phys. 36, 3256

6 - Darby, J.B. and S.T. Zegler, (1962), J. Phys. Chem. Solids, 23, 1825

7 - Forsyth, J.B. and L.M. D'Alte Da Veiga, (1963), Acta Cryst. 16 509

8 - Frank, F.C. and J.S. Kasper, (1958), Acta Cryst. 11 184

9 - Frank, F.C. and J.S. Kasper, (1959), Acta Cryst. 12 483

10 - Geller, S., B.T. Matthias, and R. Goldstein, (1955), J. Am. Chem. Soc. 77 1502

11 - Greenfield, P. and P.A. Beck, (1954), Trans. AIME, 200 253

12 - Hartly, C.S., L.D. Parsons, and J.E. Seedly, Jr., (1964), J. Met. 16 119

13 - International Tables for X-ray Crystallography (1962), Vol. III, Table 3.3.1A. Birmingham; Kynoch Press

14 - Kasper, J.S., (1956). A.S.M. Seminar on Theory of Alloy Phases, Trans. ASM, 48A 264

15 - Kasper, J.S. and R.M. Waterstrat, (1956). Acta Cryst. 9 289

16 - Matthias, B.T., (1963). Rev. Mod. Phys. 35

17 - Matthias, B.T., T.H. Gebaile, R.H. Willens, E. Corenzwit, and G.W. Hull,Jr., (1965), Phys. Rev. 139 A1501

18 - Nevitt, M.V., (1962), AIME Symposium on Electronic Structure and Alloy Chemistry of the Transition Elements, p. 123, New York, Interscience Publishers.

19 - Raub, E. and E. Röschel, (1966), Z. Metallk. 57 470

20 - Ray, A.E. and L.D. Parsons, (1966), Private Communication

21 - Rideout, S., W.D. Manly, E.L. Kamen, B.S. Lement, and P.A. Beck, (1951), Trans. AIME, 191 872

22 - Sadogopan, V., H.C. Gatos, and B.C. Giessen, (1965), J. Phys. Chem. Solids, 26 1687

23 - Spooner, F.J. and C.G. Wilson, (1964), Acta Cryst. 17 1533

24 - Sully, A.H. (1951-1952), J. Inst. Metals, 80 173

25 - Waterstrat, R.M. and E.C. van Reuth, (1966), Trans. AIME, 236 1232

26 - Wilson, C.G. (1963), Acta Cryst. 16 724

27 - Wilson, C.G. and F.J. Spooner, (1963), Acta Cryst. 16 230

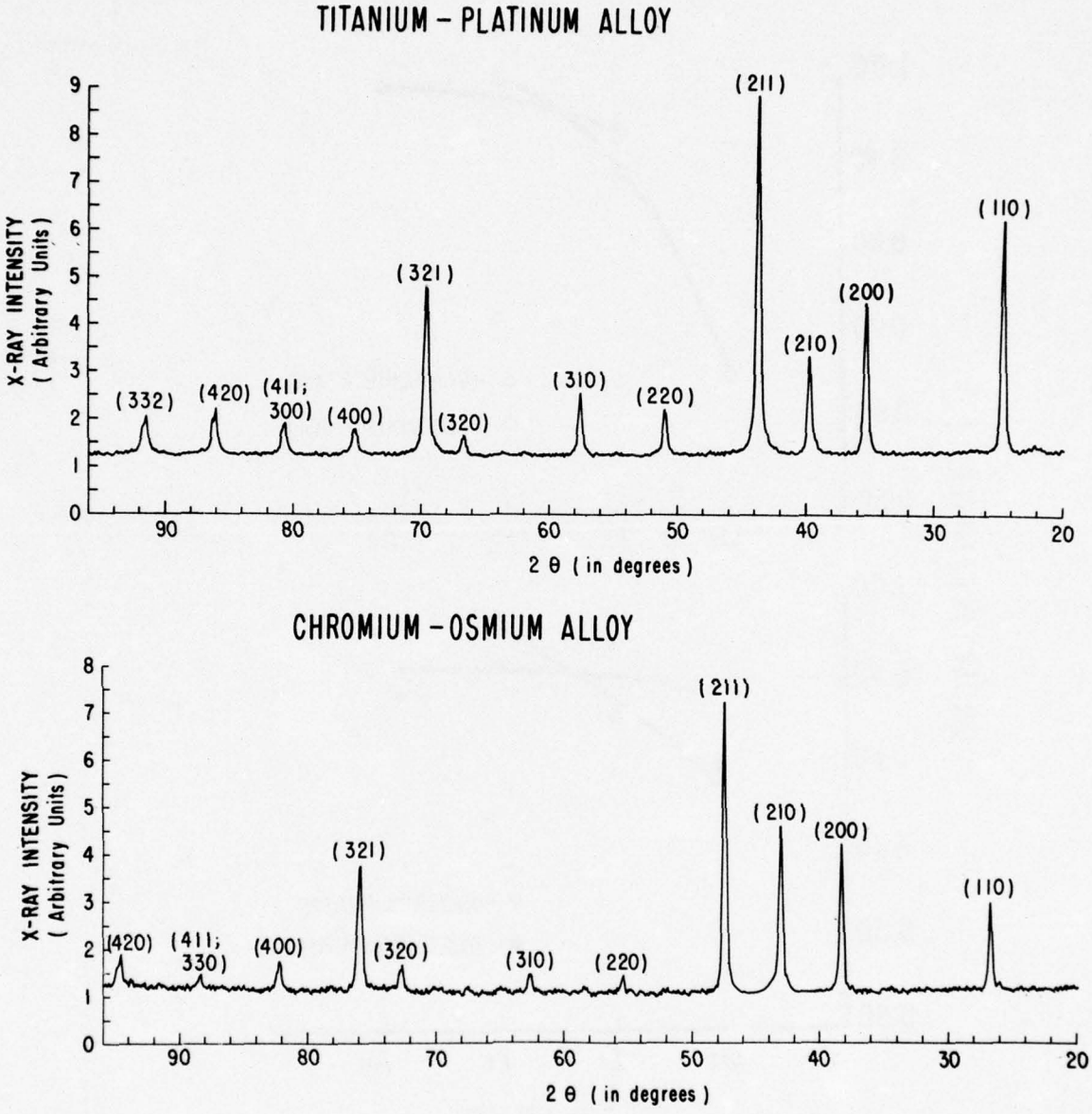

Figure 1 - X-ray Pattern of a Highly Ordered A15-Type Phase (Ti_3Pt) Compared With the Pattern of a Partially Disordered A15-Type Phase ($Cr_{72}Os_{28}$)

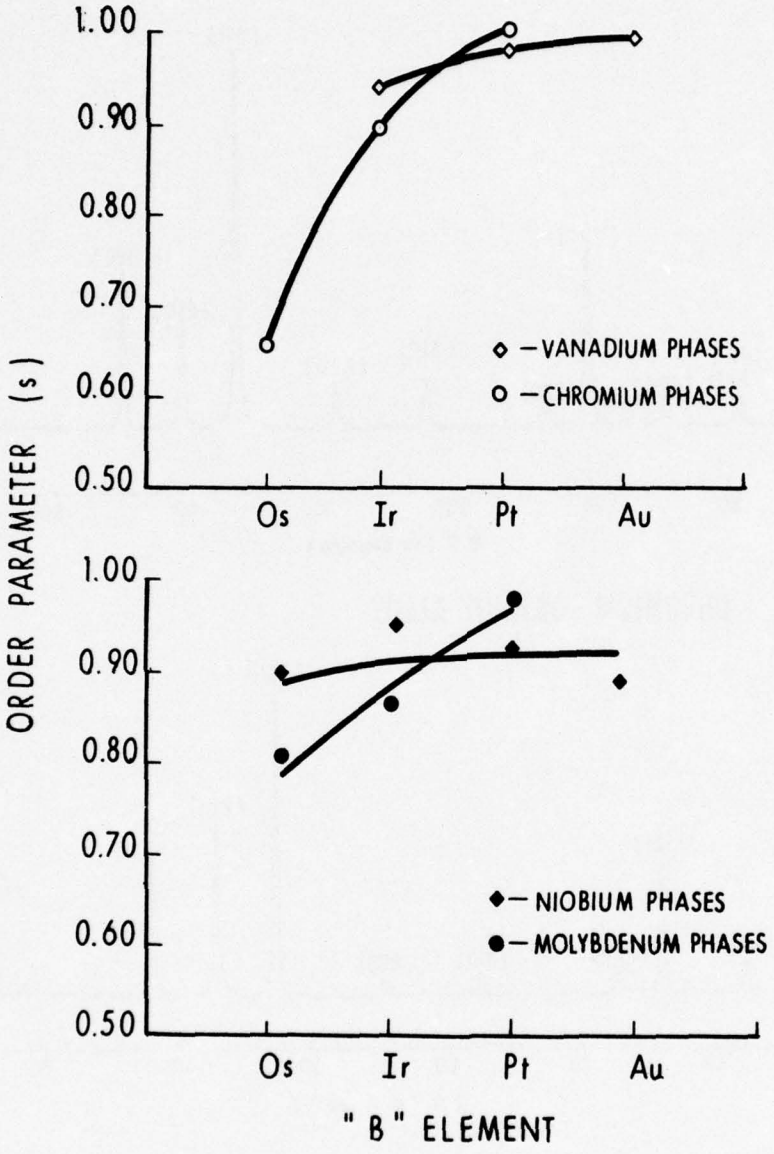

Figure 2 - Degree of Atomic Ordering in A15-Type Phases as a Function of the Position of the Constituent Elements in the Periodic Table

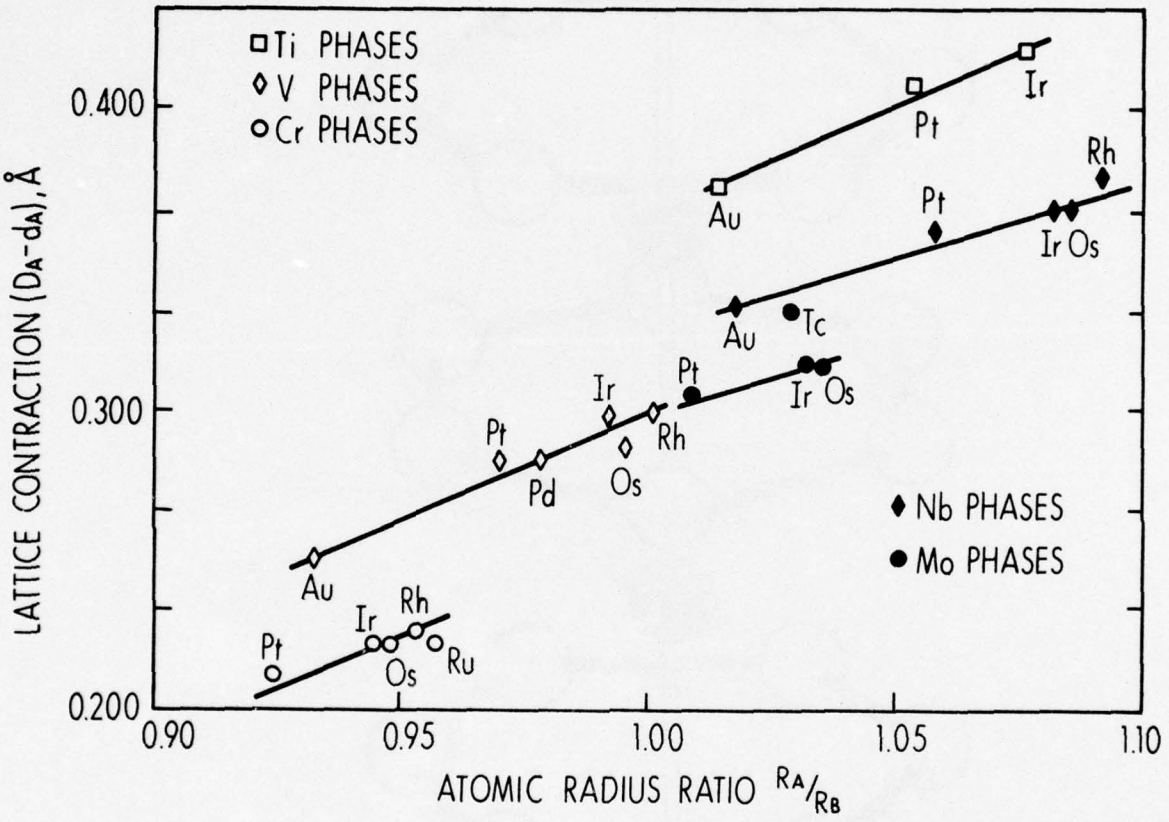

Figure 3

A-A Lattice Contractions in A15-Type Phases as a Function of the Goldschmidt Radius Ratio (R_A/R_B)

d_A = Interatomic Distance Determined from Crystallographic Data.

$R_A R_B$ = Atomic Radii Calculated from Lattice Constants of Elements Normalized to Make Values Correspond to a CN of 12. $D_A = 2R_A$

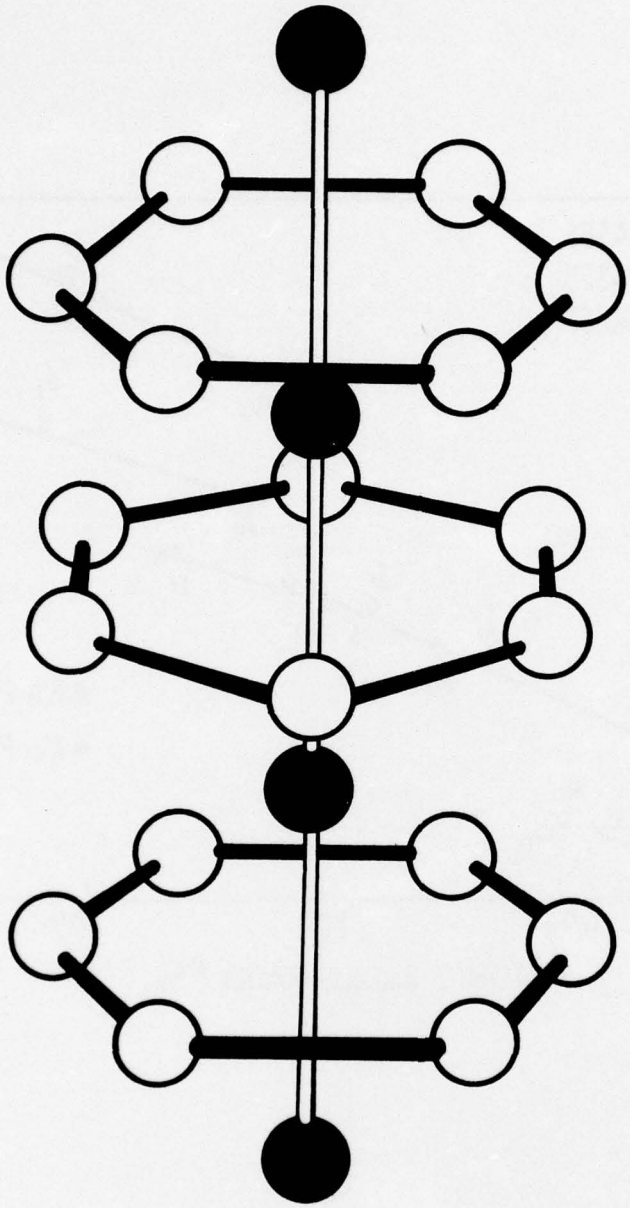

Figure 4 - Atomic Configuration Occuring in Both the Sigma and A15-Type Phases. Distances Along the Vertical A-A Atom Chain Are Exaggerated for the Sake of Clarity

Appendix A

Nomenclature

The use of the Bragg-Williams order parameter for an alloy whose composition does not correspond to the relative number of crystallographic positions in the structure (the so-called "ideal" composition) may require some justification. We have therefore made the following analysis:

We assume a binary alloy containing atoms "a" and atoms "b" where "a" and "b" identify the chemical elements present in the alloy. Let us also assume that the structure contains two crystallographic positions designated as "A-positions" and "B-positions."

Let x = the number of "b-atoms" in the B-position per unit cell,

n = the number of B-positions in the unit cell,

then $\frac{x}{n}$ = the fraction of the B-positions occupied by b-atoms

(this corresponds to r_β in the Bragg-Williams equation)

and $n - x$ the number of "a-atoms" in B-positions

(assuming that there are no vacant positions)

then hn = the number of A-positions in the unit cell.

Let y = the number of a-atoms in the A-positions per unit cell

then $hn - y$ = the number of b-atoms in the A-positions per unit cell

and $\frac{y}{hn}$ = the fraction of A-positions occupied by a-atoms

(this corresponds to r_α in the Bragg-Williams equation)

Also $hn + n$ = the total number of positions which is equal to the total number of atoms assuming there are no vacant positions.

Let F_A = the fraction of a-atoms in the alloy

F_B = the fraction of b-atoms in the alloy

then $$F_A = \frac{n - x + y}{hn + n} \quad \ldots\ldots (1)$$

$$F_B = \frac{x + hn - y}{hn + n} \quad \ldots\ldots (2)$$

The Bragg-Williams order parameter may be written

$$S_A = \frac{r_\alpha - F_A}{1 - F_A} \quad \ldots\ldots (3)$$

$$S_B = \frac{r_\beta - F_B}{1 - F_B} \quad \ldots\ldots (4)$$

where S_A and S_B are the Bragg-Williams order parameters for the A-sites and the B-sites, respectively. When $S_A = S_B$ one may of course use a single order parameter (S) to describe the ordering in the phase. It is of interest, therefore, to define the conditions under which $S_A = S_B$. Equating (3) and (4) we obtain:

$$\frac{r_\alpha - F_A}{1 - F_A} = \frac{r_\beta - F_B}{1 - F_B} \quad \ldots\ldots (5)$$

Substituting in this equation one obtains

$$\frac{\frac{y}{hn} - \left(\frac{n - x + y}{hn + n}\right)}{\frac{x + hn - y}{hn + n}} = \frac{\frac{x}{n} - \left(\frac{x + hn - y}{hn + n}\right)}{\frac{n - x + y}{hn + n}} \quad \ldots\ldots (6)$$

This may be simplified by cross-multiplication after first factoring out common denominators. Omitting detailed algebra one obtains

$$y[y - (2h - 1)n + (h - 1)x] = hx[x + (h - 2)n] - (h^2 - h)n^2 \quad \ldots(7)$$

or

$$y^2 + (h - 1)xy + (1 - 2h)yn - hx^2 - (h^2 - 2h)xn + (h^2 - h)n^2 = 0 \quad \ldots\ldots (8)$$

This equation may be factored as

$$[y + hx - hn][y - x - (h - 1)n] = 0 \quad \ldots\ldots (9)$$

Two solutions to this equation are obtained

$$y_1 = hn - hx \quad \ldots\ldots (10)$$

$$y_2 = (h - 1)n + x \quad \ldots\ldots (11)$$

This is the general solution for $S_A = S_B$ in a binary alloy phase having two crystallographic positions and assuming there are no vacant lattice sites.

For the A15-type phases; h = 3 and n = 2.

The conditions for $S_A = S_B$ can be solved by substituting these values in Equations (10) and (11) to obtain

$$y_1 = 6 - 3x \quad \ldots\ldots (12)$$

$$y_2 = 4 + x \quad \ldots\ldots (13)$$

The alloy compositions at which $S_A = S_B$ can be determined by substituting Equations (12) and (13) into Equation (1), which may be rewritten

$$(hn + n)F_A = n - x + y \quad \ldots\ldots (1a)$$

Solving in this manner one obtains

$$F_A = 1.00 - 0.50x \quad \ldots\ldots (14)$$

$$F_A = 0.75 \quad \ldots\ldots (15)$$

These solutions, of course, also define F_B since

$F_B = 1 - F_A$ by definition.

Thus,

$$F_B = 0.50x \quad \ldots\ldots (16)$$

$$F_B = 0.25 \quad \ldots\ldots (17)$$

Equation (16) requires that the fraction of "b-atoms" in the phase must be equal to one-half the number of "b-atoms" in the B-positions per unit cell. Since the B-positions contain a <u>maximum</u> of two atoms per unit cell in the A15-type phases, one-half the number of "b-atoms" in these positions is equivalent to the <u>fraction</u> of "b-atoms" in these positions. Equation (16), therefore, simply requires that any binary A15-type phase must be <u>completely disordered</u> with $S_A = S_B = 0$ <u>regardless</u> of the chemical <u>composition</u> of the

phase. Equation (17), however, requires that the composition of the A15-type phase must be restricted to the so-called "ideal" composition (A_3B) regardless of the degree of ordering.

If the Bragg and Williams order parameter is to be used for "nonideal" compositions one must therefore assign different values of this parameter to each crystallographic position. In crystal structures containing more than two crystallographic positions, or more than two components, it appears that, in general, the order parameters on the different atom sites will be unequal and, consequently, the order parameter must be defined for each position. One must use only positive values, however, since one is defining the preference of an atom for a given position and not the tendency of the atom to avoid the position.

In our computer program we adopted certain simplifying assumptions in dealing with "nonstoichiometric" compositions. In order to avoid solving for a separate order parameter on each atom site, we redefined the order parameter in a manner which differs somewhat from the usual definition as given in the Bragg-Williams equation. Our redefined order parameter retains an assigned value of zero as corresponding to a completely disordered alloy, but instead of defining S = 1 as the value for a completely ordered alloy we have defined this value as corresponding to the maximum amount of ordering possible considering the alloy composition.

In a binary nonstoichiometric alloy this simply means that the atom position which can never be completely filled by one type of atom is assigned an order parameter value of one when the position is filled to the maximum extent permitted by the alloy composition. The other position, of course, must be completely filled at this point with one atom type and its order

parameter would therefore correspond to the usual Bragg-Williams definition, or in other words, to a value of one also. Thus, by redefining the order parameter in this manner, a single order parameter suffices to describe the extent of atomic ordering on both atom sites as it varies from random occupancy to complete ordering. The computer may then obtain a single solution in terms of this redefined order parameter. The single value so obtained may subsequently be converted to separate values describing the extent of ordering on each atom site in terms of the usual Bragg-Williams definition given by Equations (3) and (4). This may be done by equating the Bragg-Williams order parameter (S_A or S_B) to a constant (K_A or K_B) times the single value obtained for the redefined order parameter (S').

Thus,

$$S_A = K_A S' \qquad \ldots\ldots (18)$$

$$S_B = K_B S' \qquad \ldots\ldots (19)$$

For a nonstoichiometric composition, either K_A or K_B must equal one, but K_A cannot be equal to K_B. One may solve for K_A or K_B using the values of S_A or S_B and the value of S' corresponding to maximum ordering. The value of S_A or S_B corresponding to a maximum ordering in the site not completely filled can be obtained using Equations (3) and (4) by using values of r_α or r_β which correspond to the maximum filling of this site.

In making these simplifications we assigned a modifying constant to the atomic form factor for the position which cannot be completely filled by one type of atom. This constant changes the form factor so that when the redefined order parameter for this position equals one, the scattering corresponds to what one would expect for the amount of dilution obtained by the partial filling. This simplification ignores the slight differences in

angular dependence of the form factor which would exist if a weighted average of each form factor were used. In the case of small deviations from the ideal stoichiometry, however, (only a few percent) this error is probably not significant and is certainly small relative to the overall experimental error. For larger deviations from the "ideal" stoichiometry, the weighted average of the two form factors must, of course, be used.

Security Classification Unclassified

DOCUMENT CONTROL DATA - R&D

(Security classification of title, body of abstract and indexing annotation must be entered when the overall report is classified)

1. ORIGINATING ACTIVITY *(Corporate author)*

U.S.Navy Marine Engineering Laboratory
Annapolis, Maryland 21402

2a. REPORT SECURITY CLASSIFICATION

U

2b. GROUP

3. REPORT TITLE

Atomic Ordering in Binary A15-Type Phases •

4. DESCRIPTIVE NOTES *(Type of report and inclusive dates)*

Research and Development Report.

5. AUTHOR(S) *(Last name, first name, initial)*

van Reuth, E.C. and Waterstrat, R.M.

E. C. Ivan Reuth
R. M. Waterstrat

6. REPORT DATE

March 1967

7a. TOTAL NO. OF PAGES

45

7b. NO. OF REFS

27

8a. CONTRACT OR GRANT NO.

b. PROJECT NO. Z-R011 01 01

c. Task 0401

d. ZR0110101

9a. ORIGINATOR'S REPORT NUMBER(S)

MEL-6/67

64 pp.

9b. OTHER REPORT NO(S) *(Any other numbers that may be assigned this report)*

Assigt 87 121

10. AVAILABILITY/LIMITATION NOTICES

Distribution of this document is unlimited

11. SUPPLEMENTARY NOTES

12. SPONSORING MILITARY ACTIVITY

13. ABSTRACT

The degree of long-range order has been determined for 20 binary A15-type phases containing various transition elements. A tendency toward a lower degree of order was noted as the component elements were chosen successively from columns in the periodic table approaching the Mn column. A comparison of the ordering in the A15-type phases with the ordering previously reported for various binary sigma phases suggests that the remarkable stability of these phases may result from an interdependence between the electronic structure and the ability of the atoms to undergo deformations in conforming to geometrical packing requirements.

(Authors)

DD FORM 1 JAN 64 1473

Unclassified
Security Classification

217150

LB

Security Classification Unclassified

14. KEY WORDS	LINK A		LINK B		LINK C	
	ROLE	WT	ROLE	WT	ROLE	WT
Crystallography						
Alloy phases						
Transition elements						
Long-range order						
Binary A-15 type phases						
Ordering						
Binary sigma phases						
Electronic structure						
Geometrical packing						
Superconductivity						
Intermetallic compounds						

Navy Marine Engineering Laboratory
Report 6/67
ATOMIC ORDERING IN BINARY A15-TYPE PHASES, by E. C. van Reuth and R.M. Waterstrat.
March 1967. 45 pp. Figs.
UNCLASSIFIED

The degree of long-range order has been determined for 20 binary A15-type phases containing various transition elements. A tendency toward a lower degree of order was noted as the component elements were chosen successively from columns in the periodic table approaching the Mn column. (over)

1. Long-range Ordering
2. A15-type Structures
3. Superconductivity
4. Transition Metals
5. Intermetallic Compounds

I. van Reuth, E.C.
II. Waterstrat, R.M.
III. Title
IV. 6/67

UNCLASSIFIED

A comparison of the ordering in the A15-type phases with the ordering previously reported for various binary sigma phases suggests that the remarkable stability of these phases may result from an interdependence between the electronic structure and the ability of the atoms to undergo deformations in conforming to geometrical packing requirements.

Navy Marine Engineering Laboratory
Report 6/67
ATOMIC ORDERING IN BINARY A15-TYPE PHASES, by E. C. van Reuth and R.M. Waterstrat.
March 1967. 45 pp. Figs.
UNCLASSIFIED

The degree of long-range order has been determined for 20 binary A15-type phases containing various transition elements. A tendency toward a lower degree of order was noted as the component elements were chosen successively from columns in the periodic table approaching the Mn column. (over)

1. Long-range Ordering
2. A15-type Structures
3. Superconductivity
4. Transition Metals
5. Intermetallic Compounds

I. van Reuth, E.C.
II. Waterstrat, R.M.
III. Title
IV. 6/67

UNCLASSIFIED

A comparison of the ordering in the A15-type phases with the ordering previously reported for various binary sigma phases suggests that the remarkable stability of these phases may result from an interdependence between the electronic structure and the ability of the atoms to undergo deformations in conforming to geometrical packing requirements.

Navy Marine Engineering Laboratory
Report 6/67
ATOMIC ORDERING IN BINARY A15-TYPE PHASES, by E. C. van Reuth and R.M. Waterstrat.
March 1967. 45 pp. Figs.
UNCLASSIFIED

The degree of long-range order has been determined for 20 binary A15-type phases containing various transition elements. A tendency toward a lower degree of order was noted as the component elements were chosen successively from columns in the periodic table approaching the Mn column. (over)

1. Long-range Ordering
2. A15-type Structures
3. Superconductivity
4. Transition Metals
5. Intermetallic Compounds

I. van Reuth, E.C.
II. Waterstrat, R.M.
III. Title
IV. 6/67

UNCLASSIFIED

A comparison of the ordering in the A15-type phases with the ordering previously reported for various binary sigma phases suggests that the remarkable stability of these phases may result from an interdependence between the electronic structure and the ability of the atoms to undergo deformations in conforming to geometrical packing requirements.

Navy Marine Engineering Laboratory
Report 6/67
ATOMIC ORDERING IN BINARY A15-TYPE PHASES, by E. C. van Reuth and R.M. Waterstrat.
March 1967. 45 pp. Figs.
UNCLASSIFIED

The degree of long-range order has been determined for 20 binary A15-type phases containing various transition elements. A tendency toward a lower degree of order was noted as the component elements were chosen successively from columns in the periodic table approaching the Mn column. (over)

1. Long-range Ordering
2. A15-type Structures
3. Superconductivity
4. Transition Metals
5. Intermetallic Compounds

I. van Reuth, E.C.
II. Waterstrat, R.M.
III. Title
IV. 6/67

UNCLASSIFIED

A comparison of the ordering in the A15-type phases with the ordering previously reported for various binary sigma phases suggests that the remarkable stability of these phases may result from an interdependence between the electronic structure and the ability of the atoms to undergo deformations in conforming to geometrical packing requirements.

850

DEPARTMENT OF THE NAVY
NAVAL SHIP RESEARCH AND DEVELOPMENT CENTER
Successor to David Taylor Model Basin and Navy Marine Engineering Laboratory
ANNAPOLIS, MARYLAND 21402

IN REPLY REFER TO

NP/10310(M870 ECV)
Assigt 87 121
Rept 6/67

ANNAPOLIS DIVISION

18 MAY 1967

From: Officer in Charge
To: Commander, Naval Ship Systems Command (SHIPS 031)

Subj: Report 6/67, Transmittal of

1. Transmitted herewith is Report 6/67, Atomic Ordering in Binary A15-Type Phases. The information contained herein was developed during the course of work, supported by the Foundational Research Program, Subproject Z-R011 01 01, Task 0401.

2. This report was prepared in the form of a manuscript submitted for publication to Acta Crystallographica.

H. C. Dalrymple

H. C. Dalrymple
By direction

Copy to:
(See Distribution List, page ii)

MEL Report 6/67

Atomic Ordering in Binary A15-Type Phases

by

E. C. van Reuth *

and

R. M. Waterstrat **

* Senior Research Scientist, U. S. Navy Marine Engineering Laboratory, Annapolis, Maryland; on leave of absence to Kamerlingh Onnes Laboratory, University of Leiden, Leiden, The Netherlands, for the 1966-67 academic year.

** Research Associate, American Dental Association, National Bureau of Standards, Washington, D.C.